Soft Matter

PAPER

View Article Online
View Journal

Cite this: DOI: 10.1039/c9sm00455f

Explosive bouncing on heated silicon surfaces under low ambient pressure

Xingjian Yu, Run Hu, Xiaoyu Zhang, Bin Xie and Xiaobing Luo *

Received 4th March 2019,
Accepted 25th April 2019

DOI: 10.1039/c9sm00455f

rsc.li/soft-matter-journal

Droplet impingement on heated surfaces has been investigated by varying the surface textures, temperature, and droplet properties with demonstration of various phenomenological behaviors, such as evaporation, boiling, splashing, and Leidenfrost bouncing. However, the ambient pressure dependence has not been well explored, especially for ambient pressures lower than 5 kPa. By examining the ambient pressure (from 0.2 to 20 kPa) and surface temperature (from 20 to 200 °C) simultaneously, we found a novel explosive bouncing behavior which is different from Leidenfrost bouncing and only occurs at extremely low ambient pressure (≤6 kPa). Through experimental validation and mechanical analysis, we found that the explosive bouncing is caused by the dramatic explosion of the local vapor bubble and reducing the ambient pressure benefits the formation and explosion of the vapor bubble.

I. Introduction

Impinging of liquid droplets on a heated solid surface has long been regarded as a paradigm to explore physical mechanisms in nature and to develop a broad range of advanced technologies, such as metal quenching,[1] droplet transportation,[2,3] spray cooling,[4–6] falling film evaporation[7] and fuel injection.[8] In general, the droplets may undergo various behaviors including evaporation,[9] boiling,[10] splashing[11,12] and Leidenfrost bouncing,[13–16] depending on the surface properties,[17–19] droplet properties,[20–22] and ambient conditions.[23–25] Among the ambient conditions, the ambient pressure was found to have influence on the Leidenfrost temperature and the efficiency of heat exchange as the liquid saturation temperature falls sharply with ambient pressure.[24,25] In recent years, researchers have devoted significant efforts to further investigate the dynamic droplet behaviors under ambient pressures from 5 kPa to atmospheric pressure using high-speed cameras.[26–28] These works further illustrate the ambient pressure dependence of the temperature boundary between the evaporation, boiling and Leidenfrost bouncing, which is of great importance for application of the liquid–surface interaction at sub-atmospheric pressure. However, as far as we are aware, there are no works on ambient pressure below 5 kPa. According to the previous studies,[27,28] the saturation temperatures of water are ~33 °C at 5 kPa and ~24 °C at 3 kPa, which results in different evaporation interactions between the droplets and the heated surface. This pressure-dependence phenomenon would be more obvious upon further reducing the ambient pressure, highlighting the importance of further investigation on the ambient pressure. Hence, we would like to explore water droplet behavior under low ambient pressure and the related mechanism in the control of droplet behaviors.

State Key Laboratory for Coal Combustion, School of Energy and Power Engineering, Huazhong University of Science and Technology, Wuhan 430074, China. E-mail: luoxb@hust.edu.cn

II. Experiments

To study the droplet behaviors under low ambient pressure, we built an experimental setup as shown in Fig. 1. A vacuum pump (EDWAROS, RV11) was applied to impose the ambient pressure P_a in a transparent acrylic chamber (250 × 250 × 250 mm) with a pressure sensor (0–100 kPa with an accuracy of 0.2%) to monitor the ambient pressure. The silicon substrate was first immersed into an acetone solution for 15 min and washed in ethanol solution three times, then dried in an oven at 50 °C for 30 minutes. A polished copper heater with a temperature

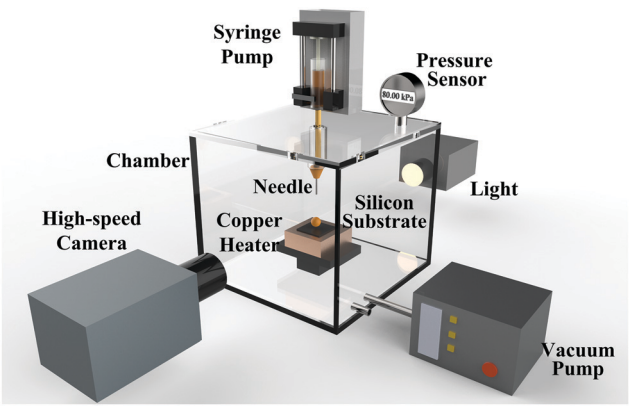

Fig. 1 Experimental setup.

control precision of ±1 °C was applied to heat the silicon substrate. Deionized water droplets with a diameter of 2 mm ± 10% were generated by pushing liquid from a syringe pump at a low rate (≈1 μl s^{-1}) into a capillary needle (inner diameter of 0.11 mm, external diameter of 0.23 mm). To minimize the inertial effect, the droplets were gently deposited onto the surface with a small Weber number ($We = \rho_l U^2 D/\gamma \approx 1$, in which ρ_l is the density of the liquid, U is the impact velocity, D is the diameter of the droplets and γ is the surface tension of the liquid) by adjusting the height of the tip of the needle to the substrate. The behavior of the droplets was captured using a high-speed camera (SA3 120K, Photron) with a resolution of 1024 × 1024 dpi against a 36 W white-light backlighting unit.

A flat polished silicon substrate with an average surface roughness of approximately 5 nm was used in the experiments. The substrate was first immersed into acetone solution for 15 min and washed in ethanol solution three times, then dried in a 50 °C oven for 30 min. The static contact angle (CA) and contact angle hysteresis (CAH) of the water droplet on the surface were measured as 68° and 33° at 25 °C. The static CA was measured using the drop shape analyzer (DSA25, Kruss) by depositing a water droplet with diameter of 2 mm onto the surface. The CAH is defined as the difference between the advancing and receding CA which were measured as 88° and 55° using the dynamic sessile drop method.[29] We repeated the water droplet impingement experiment ten times at each ambient pressure P_a (from 0.2 to 20 kPa) and surface temperature T_s (from 20 to 200 °C), and recorded the behavior of each droplet one by one.

III. Results and discussion

Fig. 2a summarizes the behavior of the droplets on the flat silicon surface under various ambient pressures and surface temperatures. It shows that besides evaporation, boiling and Leidenfrost bouncing behaviors, a novel kind of droplet behavior (the dashed region) was found under a low P_a (≤6 kPa) and moderate T_s (from 60 to 160 °C). We define this droplet behavior as explosive bouncing as it acquires the energy for bouncing from the explosion of the vapor bubble, the typical droplet behavior is shown in Fig. 2b. In comparison, Leidenfrost bouncing with the same surface overheat ($\Delta T = T_s - T_{sa}$, in which T_{sa} is the saturation temperature of the liquid) is plotted in Fig. 2c. Despite being under the same ΔT, the droplet undergoes different droplet morphologies in the explosive bouncing and Leidenfrost bouncing. We propose that the difference lies in the function of the vapor. To verify this point, we built a frustrated total internal reflection (FTIR) setup, as shown as Fig. 3a,[13,27] to record the bottom view of the droplet, which can distinguish the wetted area from the vapor bubbles. For Leidenfrost bouncing in Fig. 3b, no liquid–surface interface was observed which indicates that the vapor forms a continuous thin layer beneath the droplet. The thin vapor layer prevents the droplet from wetting the surface, therefore the droplet bounces off the surface gently. In contrast, for the explosive bouncing shown as Fig. 3c, the vapor fails to form a continuous thin layer to float the droplet, but only yields a local vapor bubble. The vapor bubble expands rapidly owing to the high surface overheat and explodes dramatically soon after the

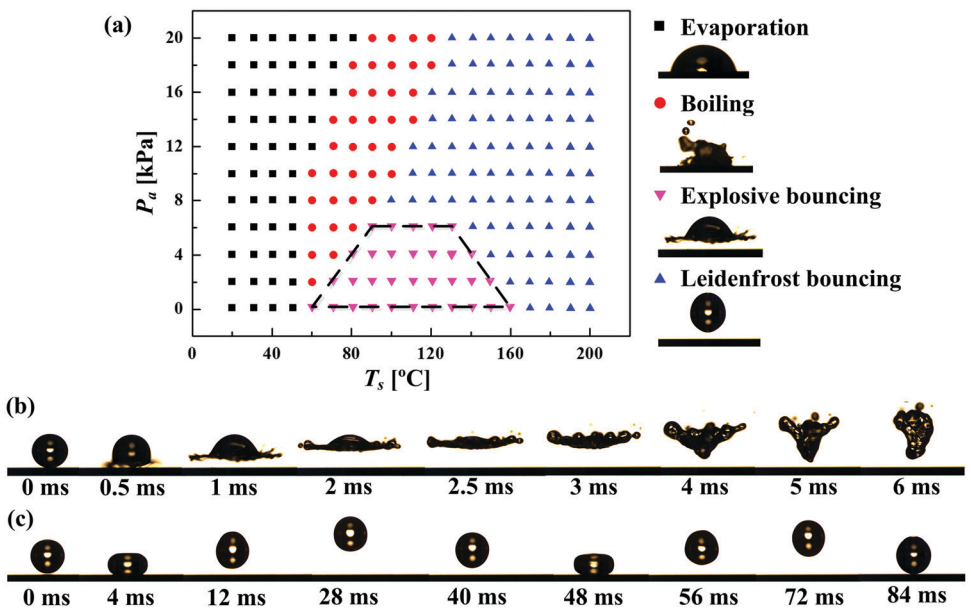

Fig. 2 (a) Phase diagram of the droplet behaviors under various ambient pressures and surface temperatures. Four typical droplet behaviors are observed, including evaporation (black square), boiling (red circle), explosive bouncing (pink lower triangle), and Leidenfrost (blue upper triangle). (b) Explosive bouncing under an ambient pressure of 4 kPa and surface temperature of 110 °C. (c) Leidenfrost bouncing under an ambient pressure of 12 kPa and surface temperature of 130 °C. The water saturation temperatures, T_{sa}, at 4 and 12 kPa are ~29 °C and ~49 °C, respectively, therefore both the surface overheat, ΔT, of explosive bouncing and Leidenfrost bouncing are ~81 °C. The water saturation temperatures are derived from ref. 30.

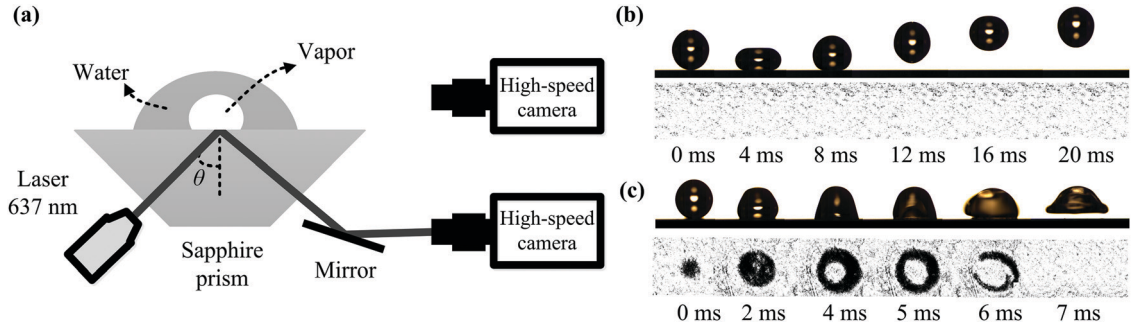

Fig. 3 (a) Schematic diagram of the FTIR setup. All of the components are placed inside the vacuum chamber shown in Fig. 1 except for the high-speed cameras. A flat transparent sapphire prism is used so that both the bottom and side views can be recorded. (b) Leidenfrost bouncing under an ambient pressure of 8 kPa and a surface temperature of 120 °C. (c) Explosive bouncing under an ambient pressure of 0.2 kPa and a surface temperature of 70 °C. The black (white) region represents the liquid–surface (vapor–surface) interface.

droplet contacts the surface, providing abundant energy to generate the explosive bouncing phenomenon.

Moreover, from Fig. 2 and 3, we can see that the ambient pressure plays an important role in determining the appearance of explosive bouncing. We propose that there are two necessary conditions for triggering explosive bouncing: (i) a sufficiently large liquid–surface contact area to provide an enclosed space for local vapor bubble formation; (ii) a sufficiently high surface overheat to generate large amounts of vapor instantly. These two conditions determine the fact that explosive bouncing can only take place under low ambient pressure and moderate surface temperature conditions. To prove this point, we conducted qualitative mechanical analysis for two typical droplet states: (i) the initial impact state shown in Fig. 4a; and (ii) the local vapor bubble accumulation state shown in Fig. 4b.

For the initial impact state shown in Fig. 4a, the droplet suffers from gravity, inertial force, vapor pressure P_{v1} and gas pressure P_g, which determines the wetting or non-wetting state of the droplet. Once the gravity and inertial force overwhelm P_{v1} and P_g, the droplet wets the surface. Otherwise, the droplet cannot wet the surface and presents Leidenfrost bouncing behavior. In our experiments, the gravity and inertial force were constant. However, the P_g is strongly related to the ambient pressure. It is reported that when a droplet falls down to the substrate, part of the gas that is confined between the droplet and substrate is compressed into a thin layer, which provides substantial pressure P_g to prevent the droplet from wetting the surface in a short or long period of time.[31,32] Obviously, P_g decreases sharply with the ambient pressure. Therefore, under low ambient pressure, it is easier for the

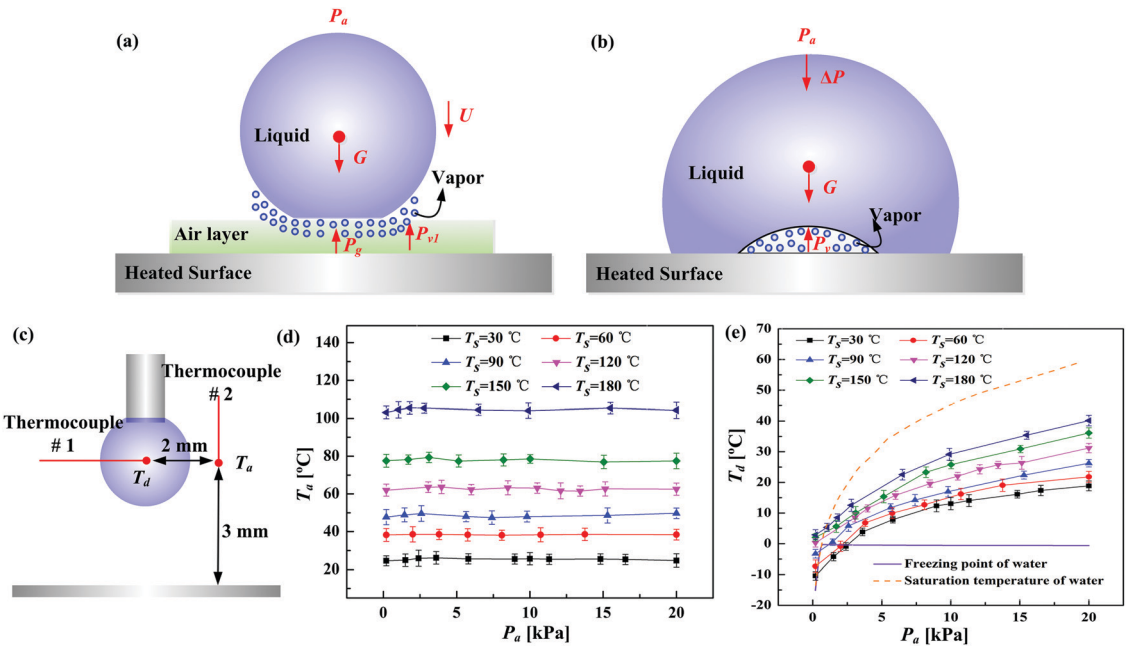

Fig. 4 Mechanical analysis of two typical impact states. (a) Initial impact state. (b) Local vapor layer accumulation state. (c) Measurement of the air temperature T_a on the droplet temperature at release T_d. (d) T_a under various ambient pressures and surface temperatures. (e) T_d under various ambient pressures and surface temperatures. The saturation temperatures and freezing points of the water were obtained from ref. 30.

droplet to wet the surface to provide an enclosed space for local vapor layer formation. The formation of P_{v1} is similar to that of P_g. Owing to the evaporation of the droplet, part of the vapor that is confined between the droplet and the substrate is compressed into a thin layer, which contributes to the formation of P_{v1}. Therefore, the P_{v1} is strongly related to the temperature difference between the droplet temperature and the water saturation temperature. In the experiments, the initial temperature of the water was close to 25 ± 1 °C. However, it takes approximately 15 s for the water to accumulate and release from the needle, resulting in a temperature variation in water owing to the interplay between the evaporation and heat transfer from the heated surface and the surrounding air. Therefore, we measured the droplet temperature T_d at release and the air temperature T_a around the droplet using two tiny thermocouples (TT-K-36-SLE with diameter of 0.1 mm, Omega) as shown in Fig. 4c. Fig. 4d and e show the T_a and T_d under various ambient pressures and surface temperatures. It shows that the T_a increases with the T_s but barely changes with the P_a. In addition, the T_a is much higher than the T_d, which indicates that the droplet can be sufficiently heated by the surrounding air. Owing to the heating process and low ambient pressure, the droplet evaporates and takes heat from the water itself. As a result, the T_d drops below its initial temperature for the majority of the conditions. Moreover, Fig. 4e shows that the T_d varies from −10 to 40 °C as the P_a and T_s changes. However, freezing rarely occurs as the droplet temperature is lower than the freezing point of water in only a few conditions. Moreover, as we used pure deionized water and there is almost no dust and impurities in the vacuum chamber under low ambient pressure, the water can remain subcooled owing to the lack of the crystal nucleus that is required for freezing. The T_d is very important for determining the P_{v1}. As shown in Fig. 4e, the T_d increases with the T_s, which increases the P_{v1} owing to the higher temperature difference between the T_d and water saturation temperature. Under a high surface temperature, the P_{v1} would be large enough to prevent the droplet from wetting the surface, even the when the P_g is approximately 0 under an ultra-low ambient pressure. Therefore, no explosive bouncing was observed when the surface temperature was higher than 170 °C, as shown in Fig. 2a.

After the droplet wets the surface, the local vapor layer generates and accumulates at the liquid–substrate contact surface, as shown in Fig. 4b. The vapor explodes violently and levitates the droplet if P_v overwhelms the capillary pressure ΔP, gravity and ambient pressure P_a. Otherwise, the vapor bubble explodes gently and fails to levitate the droplet, which is known as a boiling phenomenon.

The vapor pressure P_v can be calculated by establishing the mass conservation equation of vapor. After the droplet contacts with the surface for time t, the mass of the generated vapor can be calculated as:

$$m_{vapor} = \int_0^t \frac{qA}{h_{fg}} dt \quad (1)$$

In which q is the heat flux from the hot surface, h_{fg} is the latent heat of vaporization, t is residence time and A is the area of the contact surface. The heat flux q can be expressed as:[33]

$$q = k_{eff}\Delta T/e \quad (2)$$

In which k_{eff} is effective thermal conductivity, e is the effective thickness of the vapor and ΔT is the surface overheat.

By introducing the ideal gas equation, the P_v can be expressed as:

$$P_v = \frac{m_{vapor}RT}{MV_{vapor}} = \frac{\int_0^t RT\frac{k_{eff}A\Delta T}{h_{fg}e}dt}{MV_{vapor}} \quad (3)$$

In which R is the universal gas constant, T is the temperature of the vapor, M is the molecular molar mass of the vapor and V_{vap} is the volume of the vapor bubble. It shows that the vapor pressure increases with the surface overheat ΔT, contact area (contact line) A and residence time t.

The characteristic curvature of the interface leads to a capillary pressure $\Delta P \sim 2\gamma/r$, in which the r represents the curvature of the interface. The maximum capillary pressure can be calculated as $\Delta P_{max} \approx 2 \times 0.072/0.001 = 144$ Pa, which is much smaller than the ambient pressure. Therefore, reducing the ambient pressure can significantly decrease the critical pressure for the explosion of the vapor bubble.

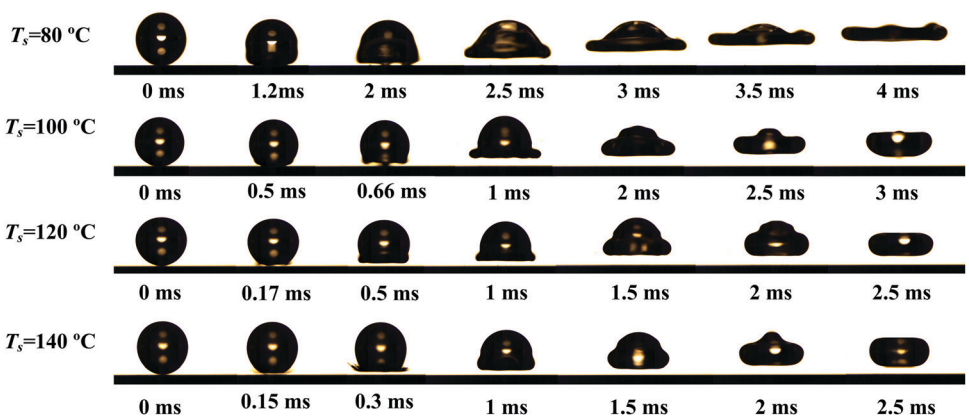

Fig. 5 Explosive bouncing on flat silicon surface under a P_a of 0.2 kPa and different surface temperatures.

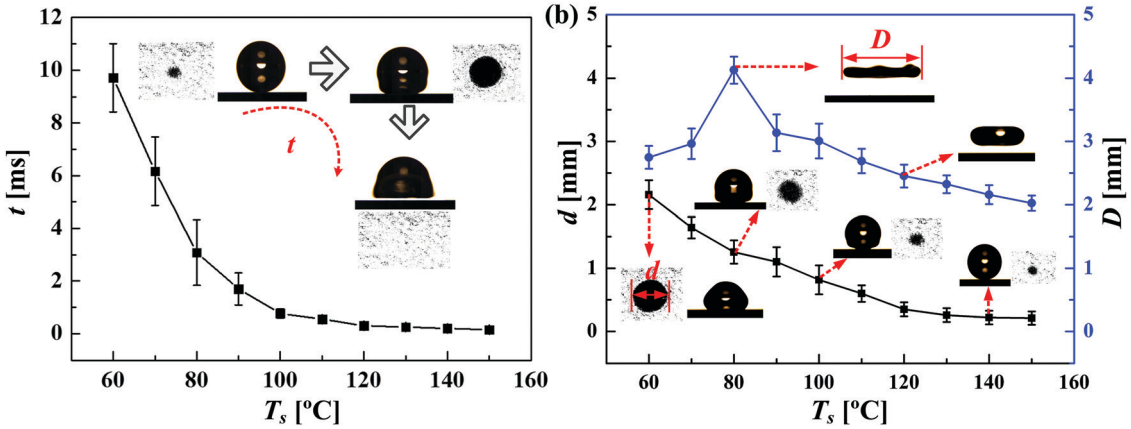

Fig. 6 (a) T_s–t and (b) T_s–d, T_s–D relationships under an ambient pressure of 0.2 kPa.

In summary, reducing the ambient pressure benefits explosive bouncing in two ways: (i) making it easier for the droplet to wet the surface under high ΔT and contribute to the formation of the local vapor bubble; and (ii) decreasing the critical pressure for the explosion of vapor bubble.

Fig. 5 shows the explosive bouncing on a flat silicon surface under an ambient pressure of 0.2 kPa and different surface temperatures. In contrast to the Leidenfrost bouncing shown in Fig. 2c, the droplet deformation of explosive bouncing is strongly related to the P_a and T_s. For Leidenfrost bouncing, the thin vapor layer simply acts as a barrier to prevent the droplet from wetting the surface, therefore the droplet bounces under the conversion of its own kinetic energy, surface energy and potential energy. As a result, the droplet deformation (such as the maximum deformation diameter and bouncing height shown in Fig. 2c and 3b) is predictable and barely changes with the P_a and T_s. However, for explosive bouncing, the droplet obtains its bouncing energy from the explosion of the local vapor bubble, which is violent and metastable. Therefore, the droplet deformation changes with P_a and T_s significantly. To quantitatively characterize the droplet deformation of explosive bouncing, we measured the residence time t, maximum contact diameter d and maximum deformation diameter D and the results are shown in Fig. 6. The residence time t is defined as the duration of time from the initial contact to the initial pop-up state and the definitions of d and D are shown in Fig. 6b. As the explosion of the vapor bubble disrupts the lower-part of the droplet and pushes the droplet to move away from the center of the droplet, the maximum deformation diameter D appears after the droplet bounces off the surface. t and d monotonously decrease with T_s which can be easily understood as a higher T_s leads to a higher rate of vapor generation and quicker accumulation of vapor. Compared to the t and d, the D presents a non-monotonous relationship with T_s. The D is mainly determined by the amount of energy that is transferred from the vapor bubble explosion to the lower-part of the droplet. There are two key factors affecting the energy transfer: (i) d, a larger d means more of the droplet gains kinetic energy from the explosion of the vapor bubble; (ii) T_s, a higher T_s leads to a more violent vapor bubble explosion which transfers more energy to the unit mass droplet. Although the vapor bubble explosion is faster and more violent with a higher T_s, the d monotonously decreases as the T_s increases. As a result, the D increases before a T_s of 80 °C and decreases afterwards.

IV. Conclusion

In summary, we experimentally investigated the behavior of water droplets on a heated flat silicon surface under a low ambient pressure. In addition to evaporation, boiling, and Leidenfrost bouncing, a novel explosive bouncing behavior was observed under low ambient pressure ($\leq$6 kPa) and moderate surface temperature (from 60 to 160 °C). The underlying physics was further analyzed using qualitative mechanical analysis. The present study supplements a feasible strategy to control droplet impingement behaviors on heated surfaces, which could highlight further applications of liquid–surface interactions at low ambient pressures.

Conflicts of interest

There are no conflicts to declare.

Acknowledgements

The authors would like to acknowledge the financial support by National Natural Science Foundation of China (51625601, 51576078, and 51606074), the Ministry of Science and Technology of the People's Republic of China (Project No. 2017YFE0100600), the financial support from Creative Research Groups Funding of Hubei Province (2018CFA001).

References

1 M. Pasandideh-Fard, S. D. Aziz, S. Chandra and J. Mostaghimi, Cooling effectiveness of a water drop impinging on a hot surface, *Int. J. Heat Fluid Flow*, 2001, **22**, 201.
2 H. Linke, B. J. Alemán, L. D. Melling, M. J. Taormina, M. J. Francis, C. C. Dow-Hygelund, V. Narayanan, R. P. Taylor and

A. Stout, Self-propelled Leidenfrost droplets, *Phys. Rev. Lett.*, 2006, **96**, 154502.
3 C. N. Baroud, F. Gallaire and R. Dangla, Dynamics of microfluidic droplets, *Lab Chip*, 2010, **10**, 2032.
4 G. Liang and I. Mudawar, Review of spray cooling – Part 2: High temperature boiling regimes and quenching applications, *Int. J. Heat Mass Transfer*, 2017, **115**, 1206.
5 G. Liang and I. Mudawar, Review of spray cooling – Part 1: Single-phase and nucleate boiling regimes, and critical heat flux, *Int. J. Heat Mass Transfer*, 2017, **115**, 1174.
6 W. Cheng, W. Zhang, H. Chen and L. Hu, Spray cooling and flash evaporation cooling: the current development and application, *Renewable Sustainable Energy Rev.*, 2016, **55**, 614.
7 S. Shen, G. Liang, Y. Guo, R. Liu and X. Mu, Heat transfer performance and bundle-depth effect in horizontal-tube falling film evaporators, *Desalin. Water Treat.*, 2013, **51**, 830.
8 M. R. O. Panão and A. L. N. Moreira, Flow characteristics of spray impingement in PFI injection systems, *Exp. Fluids*, 2005, **39**, 364.
9 C. M. Weickgenannt, Y. Zhang, A. N. Lembach, I. V. Roisman, T. Gambaryan-Roisman, A. L. Yarin and C. Tropea, Non-isothermal drop impact and evaporation on polymer nanofiber mats, *Phys. Rev. E: Stat., Nonlinear, Soft Matter Phys.*, 2011, **83**, 036305.
10 T. Tran, H. J. J. Staat, A. Prosperetti, C. Sun and D. Lohse, Drop impact on superheated surfaces, *Phys. Rev. Lett.*, 2012, **108**, 036101.
11 H. J. J. Staat, T. Tran, B. Geerdink, G. Riboux, C. Sun, J. M. Gordillo and D. Lohse, Phase diagram for droplet impact on superheated surfaces, *J. Fluid Mech.*, 2015, **779**, R3.
12 L. Xu, W. W. Zhang and S. R. Nagel, Drop Splashing on a Dry Smooth Surface, *Phys. Rev. Lett.*, 2005, **94**, 184505.
13 M. Shirota, M. A. J. Van Limbeek, C. Sun, A. Prosperetti and D. Lohse, Dynamic Leidenfrost Effect: Relevant Time and Length Scales, *Phys. Rev. Lett.*, 2016, **116**, 064501.
14 D. Quéré, Leidenfrost Dynamics, *Annu. Rev. Fluid Mech.*, 2013, **45**, 197.
15 M. A. J. Van Limbeek and M. H. K. Schaarsberg, Leidenfrost drops cooling surfaces: theory and interferometric measurement, *J. Fluid Mech.*, 2017, **827**, 614.
16 J. C. Burton, A. L. Sharpe, R. C. A. Van Der Veen, A. Franco and S. R. Nagel, Geometry of the vapor layer under a Leidenfrost drop, *Phys. Rev. Lett.*, 2012, **109**, 074301.
17 H. Kim, B. Truong, J. Buongiorno and L. W. Hu, On the effect of surface roughness height, wettability, and nanoporosity on Leidenfrost phenomena, *Appl. Phys. Lett.*, 2011, **98**, 083121.
18 H. Nair, H. J. J. Staat, T. Tran, A. van Houselt, A. Prosperetti, D. Lohse and C. Sun, The Leidenfrost temperature increase for impacting droplets on carbon-nanofiber surfaces, *Soft Matter*, 2014, **10**, 2102.
19 T. Tran, H. J. J. Staat, A. Susarrey-Arce, T. C. Foertsch, A. van Houselt, H. J. G. E. Gardeniers, A. Prosperetti, D. Lohse and C. Sun, Droplet impact on superheated micro-structured surfaces, *Soft Matter*, 2013, **9**, 3272.
20 G. Castanet, O. Caballina and F. Lemoine, Drop spreading at the impact in the leidenfrost boiling, *Phys. Fluids*, 2015, **27**, 063302.
21 J. H. Moon, D. Y. Kim and S. H. Lee, Spreading and receding characteristics of a non-Newtonian droplet impinging on a heated surface, *Exp. Therm. Fluid Sci.*, 2014, **57**, 94.
22 F. Moreau, P. Colinet and S. Dorbolo, Leidenfrost explosions, *Phys. Fluids*, 2013, **25**, 091111.
23 G. Liang and I. Mudawar, Review of drop impact on heated walls, *Int. J. Heat Mass Transfer*, 2017, **106**, 103.
24 P. Testa and L. Nicotra, Influence of Pressure on the Leidenfrost Temperature and on Extracted Heat Fluxes in the Transient Mode and Low Pressure, *J. Heat Transfer*, 1986, **108**, 916.
25 G. S. Emmerson, The effect of pressure and surface material on the leidenfrost point of discrete drops of water, *Int. J. Heat Mass Transfer*, 1975, **18**, 381.
26 F. Celestini, T. Frisch and Y. Pomeau, Room temperature water Leidenfrost droplets, *Soft Matter*, 2013, **9**, 9535.
27 M. A. J. Van Limbeek, P. B. J. Hoefnagels and M. Shirota, Boiling regimes of impacting drops on a heated substrate under reduced pressure, *Phys. Rev. Fluids*, 2018, **3**, 053601.
28 D. Orejon, K. Sefiane and Y. Takata, Effect of ambient pressure on Leidenfrost temperature, *Phys. Rev. E: Stat., Nonlinear, Soft Matter Phys.*, 2014, **90**, 053012.
29 C. Yuan, M. Huang, X. Yu, Y. Ma and X. Luo, A simple approach to fabricate the rose petal-like hierarchical surfaces for droplet transportation, *Appl. Surf. Sci.*, 2016, **385**, 562.
30 L. Hou, *Photothermal studies of single molecules and gold nanoparticles: vapor nanobubbles and conjugated polymers*, Doctoral dissertation, Leiden University, 2016.
31 J. De Ruiter, R. Lagraauw, D. Van Den Ende and F. Mugele, Wettability-independent bouncing on flat surfaces mediated by thin air films, *Nat. Phys.*, 2015, **11**, 1.
32 N. Yi, B. Huang, L. Dong, X. Quan, F. Hong, P. Tao, C. Song, W. Shang and T. Deng, Temperature-Induced Coalescence of Colliding Binary Droplets on Superhydrophobic Surface, *Sci. Rep.*, 2014, **4**, 4303.
33 H. M. Kwon, J. C. Bird and K. K. Varanasi, Increasing Leidenfrost point using micro-nano hierarchical surface structures, *Appl. Phys. Lett.*, 2013, **103**, 201601.

